Available online at www.sciencedirect.com

ScienceDirect

IFAC Papers Online CONFERENCE PAPER ARCHIVE

IFAC PapersOnLine 53-2 (2020) 14444–14449

On Optimal Control of Multichamber Suspensions

Stefano Dattilo *, **Giulio Panzani** *, **Matteo Corno** *, **Sergio M. Savaresi** *

* *Dipartimento di Elettronica, Informazione e Bioingegneria, Politecnico di Milano, Piazza L. Da Vinci 32, 20133 Milano, Italy*
e-mail: giulio.panzani@polimi.it

Abstract: This paper deals with the technological analysis, and optimal control of multichamber suspensions for automotive applications. Multichamber suspensions are composed by a variable damping shock absorber and an air-spring equipped with at least an auxiliary volume. The auxiliary volume is connected to the air-spring main chamber through a two-state valve. This configuration allows for a rapid change of both the damping and the stiffness of the suspension. The first goal of this paper is to model and analyze the behaviour of the suspension, the second goal is to investigate the potential benefit of this architecture from the comfort point of view. To this aim, the paper proposes an optimal benchmark controller and tests it in simulation showing comfort improvements up to 16% with respect to state-of-the-art solution of a passive soft spring and semi-active damping control.

Keywords: Multichamber suspension, semi-active suspension, air-spring with auxiliary volume, exhaustive search optimization, optimal control.

1. INTRODUCTION

Electronically controllable suspensions are subject of intensive research in both academy and industry. Most of the available works focus on two technologies: active and semi-active suspensions. Active suspensions, being capable of actively controlling the suspension force, outperform semi-active suspensions. They however require a complex hardware and absorb high power. Currently, semi-active suspensions, modulating the damping coefficient, offer a more reasonable performance-cost trade-off and are the preferred technology (see Savaresi et al. (2010) for an overview).

Recent technological advances have lead to the development of reactive suspensions. This class of suspensions is characterized by the possibility of electronically modulating the stiffness coefficient. To the best of the authors' knowledge, these suspensions are still under-explored in the open scientific literature. Some works study the benefit of reactive suspension in an ideal settings (Youn and Hac (1995), Spelta et al. (2011)); while others focus on designing mechanical structures to implement reactive suspensions. For example, Anubi and Crane (2015) propose an architecture composed of two variable dampers acting in orthogonal directions, that is able to modify the suspension equivalent stiffness.

This paper focuses on the multichamber suspension architecture. This kind of suspension is equipped with a variable damping shock absorber and an air-spring with an auxiliary volume. The auxiliary volume is connected to the air-spring main chamber through a two-state electronic valve. By changing the state of the valve, one can rapidly modify the stiffness coefficient without introducing active power. Multichamber suspensions seem to be the most industrially promising technology as they inherit many advantages of semi-active suspensions: low energy demand, intrinsic failproof behaviour, and mechanical simplicity.

In particular, this paper quantitatively analyses the potential of this type of suspension in improving vertical ride comfort. To this aim, we first derive a control-oriented model; we then use the model to design a full-knowledge optimal control that modulates the air-spring valve to minimize the vertical sprung mass accelerations. While not immediately implementable, this control strategy serves as a performance benchmark and allows the designer to better quantify the benefit of this technology. Two other control strategies help quantifies the effect of the specific features of the multichamber architecture. For brevity's sake, the paper focuses on constant speed straight driving.

The paper is organized as follows. Section 2 provides a mathematical model of the multichamber suspension. Section 3 formulates and solves the optimization problem. Eventually, Section 4 quantifies the performance with a simulation study.

2. SYSTEM MODELLING

2.1 Multichamber suspension modelling

The multichamber suspension is composed by a dissipative element and an elastic element. The dissipative element is a standard two-state electro-hydraulic shock-absorber: it can be set to minimum damping c_{min}, or maximum damping c_{max}, with a switching bandwidth of 40 Hz. The

10.1016/j.ifacol.2020.12.1444

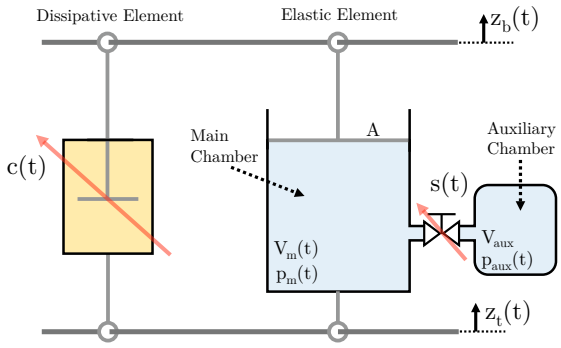

Fig. 1: Schematic representation of the multichamber suspension.

peculiarity of the multichamber suspension lies in its elastic element: the elastic force is generated by an air-spring with an additional volume. The main chamber is connected to an auxiliary chamber through a two-state electronic valve. The state of the valve determines the amount of volume available for the air compression/expansion. Figure 1 shows a schematic representation of the multichamber suspension.

The suspension force $F_s(t)$ is the sum of the damping force $F_c(t)$, and the elastic force $F_k(t)$, generated by the air-spring.

The dissipative element is modelled as:

$$\begin{aligned} \dot{c}(t) &= -\beta c(t) + \beta c_{in}(t) \\ F_c(t) &= c(t)(\dot{z}_b(t) - \dot{z}_t(t)) \end{aligned} \tag{1}$$

where β is the bandwidth of the damping dynamics, $c(t)$ and $c_{in}(t)$ are the actual and the requested damping coefficients of the shock-absorber, $z_b(t)$ and $z_t(t)$ are the position variation (with respect to the static condition) of the car body and the tire respectively, then $(\dot{z}_b(t) - \dot{z}_t(t))$ is the suspension stroke rate.

The elastic force is generated by the air-spring. Assuming an adiabatic transformation, the equivalent (*i.e* linearised around a working condition $(\bar{p},\bar{V})$) stiffness of a classic (single-chamber) air spring is:

$$k := \frac{\partial F}{\partial z} = -\frac{n\bar{p}A^2}{\bar{V}} \tag{2}$$

where A is the piston area, n is the adiabatic coefficient, $\bar{p}$ and $\bar{V}$ are the gas pressure and volume. From (2) it can be seen that, by changing the air-spring volume, the local stiffness of the spring can be varied; in particular, the larger the volume, the lower the stiffness. The multichamber suspension exploits this idea, by changing the available volume connecting/isolating the auxiliary chamber to the main one by means of a controllable valve. However, the multichamber behaviour cannot be described by the sole equation (2), as it is affected by complex dynamics, requiring a more detailed description.

In the closed valve configuration, the pressure dynamics of the two chambers is:

$$\begin{aligned} \dot{p}_m(t) &= -\frac{np_m(t)A(\dot{z}_b(t) - \dot{z}_t(t))}{V_m(t)} \\ \dot{p}_{aux}(t) &= 0 \end{aligned} \tag{3}$$

where $p_m(t)$ and $V_m(t)$ refer to pressure and volume of the main chamber, $p_{aux}(t)$ is the pressure of the auxiliary chamber that, thanks to the adiabatic assumption, does not change. Notice that the volume of the main chamber depends on the piston position, as in

$$V_m(t) = V_{m0} + A(z_b(t) - z_t(t)), \tag{4}$$

where V_{m0} is the main chamber volume in the static position.

In the open valve configuration, the system dynamics become

$$\begin{aligned} \dot{p}_m(t) &= -\frac{np_m(t)A(\dot{z}_b(t) - \dot{z}_t(t))}{V_m(t) + V_{aux}} \\ p_{aux}(t) &= p_m(t). \end{aligned} \tag{5}$$

In both configurations, the spring force is

$$F_k(t) = (p_m(t) - p_{atm})A. \tag{6}$$

where p_{atm} is the atmospheric pressure.

Figure 2 shows the air-spring mechanical characteristic for the two constant configurations (open and closed valve). The force F_0 generated at $(z_b(t) - z_t(t)) = 0$ is called static force, it is generated by the initial pressure of the system p_{m0}, and it is the force that supports the vehicle static load.

$$F_0 = (p_{m0} - p_{atm})A. \tag{7}$$

From figure, it can be clearly seen that the open valve configuration yields a lower stiffness than the closed valve one.

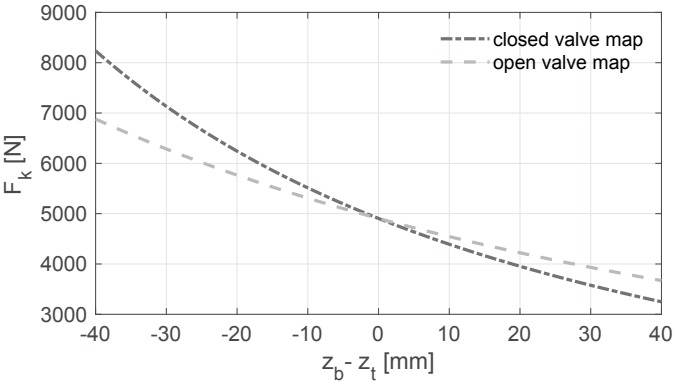

Fig. 2: Air-spring force-stroke characteristic.

The above models describe the air-spring force in either of two configurations. When a valve switch occurs special care has to be taken to model its effects. To better understand how the switching dynamics affect the air-spring characteristic, let's consider a blocked piston, closed valve and pressure in the main chamber different from the pressure in the auxiliary one. If the valve is opened, the pressure difference generates a mass exchange between the two chambers, and, after a transient, the system will reach a new steady state condition. Under the assumptions:

Assumption 1. Infinitely fast fluid dynamics transients.

Assumption 2. Negligible valve pressure drop.

Assumption 3. Instantaneous valve switch

and by defining $\bar{t}$ the valve switching instant, $\bar{t}^-$ and $\bar{t}^+$ respectively the left and right time limit to $\bar{t}$, the two

chambers will instantaneously reach the same equilibrium pressure

$$\begin{aligned} p_m(\bar{t}^+) &= p^{eq}(\bar{t}^-) \\ p_{aux}(\bar{t}^+) &= p^{eq}(\bar{t}^-) \end{aligned} \tag{8}$$

where the equilibrium pressure $p^{eq}(t)$ is

$$p^{eq}(t) = \frac{p_m(t)V_m(t) + p_{aux}(t)V_{aux}}{V_m(t) + V_{aux}}. \tag{9}$$

After the valve switching, defining the valve state $s(t)$ as:

$$s(t) = \begin{cases} 1 & \text{open valve} \\ 0 & \text{closed valve} \end{cases} \tag{10}$$

the two pressures follow the dynamic represented by

$$\begin{aligned} \dot{p}_m(t) &= -\frac{np_m(t)A(\dot{z}_b(t) - \dot{z}_t(t))}{V_m(t) + s(t)V_{aux}} \\ \dot{p}_{aux}(t) &= -\frac{np_{aux}(t)A(\dot{z}_b(t) - \dot{z}_t(t))}{V_m(t) + V_{aux}}s(t) \end{aligned} \tag{11}$$

In practice, the system is modelled as a discontinuous system. The valve opening leads to a system resetting, the equilibrium pressure is the *new* initial condition of both chambers pressure, and then the two pressures follow the dynamics derived in case of open valve. Since the two pressures start from the same initial condition $p_{m0} = p_{aux0} = p^{eq}(\bar{t}^-)$, equation (11) guarantees that the pressure of the main and auxiliary chamber will be the same until a valve closing occurs.

When the valve is closed the auxiliary chamber is isolated, and its pressure remains constant. The pressure of the main chamber changes its dynamics since the total volume is reduced to the volume of the main chamber only. This behaviour is already well represented by equation (11), without the necessity of a system resetting.

It is important to remark that, every time a valve switching occurs, the system starts from a new initial condition. More precisely:

$$\begin{aligned} &\text{if } s(\bar{t}^-) = 0 \wedge s(\bar{t}^+) = 1 \quad \rightarrow \begin{cases} p_{m0} = p^{eq}(\bar{t}^-) \\ p_{aux0} = p^{eq}(\bar{t}^-) \\ c_0 = c(\bar{t}^-) \end{cases} \\ &\text{if } s(\bar{t}^-) = 1 \wedge s(\bar{t}^+) = 0 \quad \rightarrow \begin{cases} p_{m0} = p_m(\bar{t}^-) \\ p_{aux0} = p_{aux}(\bar{t}^-) \\ c_0 = c(\bar{t}^-) \end{cases} \end{aligned} \tag{12}$$

2.2 Air-spring behaviour analysis

Section 2.1 showed that the multichamber architecture can change the equivalent stiffness of the suspension. However the behaviour is far from the ideal behaviour of a spring with a controllable stiffness. A spring with an ideal controllable stiffness coefficient can be represented as:

$$F_k(t) = k(t)(z_b(t) - z_t(t)) + F_{pre} \tag{13}$$

where $k(t) \in \{k_1, k_2\}$ is the controllable stiffness, and F_{pre} is the force due to the suspension preload.

The main difference is in the immediate effect of a switch. Considering the *ideal model*, every stiffness switch generates a force discontinuity that depends only on the suspension stroke $(z_b(t) - z_t(t))$. The air-spring with additional volume generates a force discontinuity (kick force) only in case of a valve opening, but not in case of a valve closing. Moreover, the force change due to a valve opening depends on the chambers pressure, which are influenced by the system evolution; differently, considering the *ideal model*, the force discontinuity depends only on the suspension stroke, regardless the previous system evolution.

Another important difference is in the suspension static position. The *ideal model* generates the static force at $z_b(t) - z_t(t) = 0$ regardless of the value of the controllable stiffness; as a consequence, the suspension static position never changes. On the other hand, the air-spring with an additional volume may change its static position. Consider the system at steady state and the air-spring valve open, in this condition, the air-spring force balances the sprung mass load. If the piston moves from the equilibrium position and then a valve switch takes place, the air-spring force characteristic changes.

Figure 3 exemplifies these considerations: starting from the static position $z_b(t) - z_t(t) = 0$ with open valve, the suspension is compressed, the evolution is represented by the line with circle marker. At $(z_b(\bar{t}) - z_t(\bar{t})) = -20$ mm the valve is closed, after the switch the evolution is represented by the line with square marker.

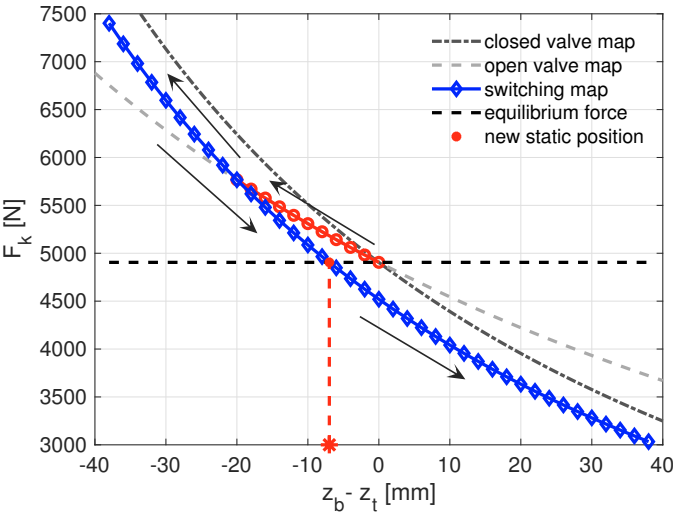

Fig. 3: Air-spring force characteristic and example of evolution.

The static force is generated in a different piston position: $(z_b - z_t) = -7$ mm, it means that the piston equilibrium position is changed.

Based on the above considerations, it is clear that the multichamber suspension cannot be modelled as an ideal variable stiffness element.

2.3 Quarter car model

This work focuses on the comfort improvement that a multichamber suspension can bring to a vehicle during straight driving at constant speed. The quarter car model accurately describes the vertical dynamics in these conditions. Figure 4 recalls the quarter car model:

$$\begin{aligned} M\ddot{z}_b(t) &= \delta F_s(t) \\ m\ddot{z}_t(t) &= -\delta F_s(t) - k_t(z_t(t) - z_r(t)). \end{aligned} \tag{14}$$

M and m are the quarter car body mass (sprung mass) and the unsprung mass respectively. $z_r(t)$ represents the road profile disturbance. k_t is the tire stiffness. $\delta F_s(t)$ is the multichamber suspension dynamic force, and it is defined as:

$$\delta F_s(t) = F_s(t) - F_0 \tag{15}$$

where $F_s(t)$ is the force generated by the suspension, and F_0, as in (6) is the static force. Overall, the dynamics of

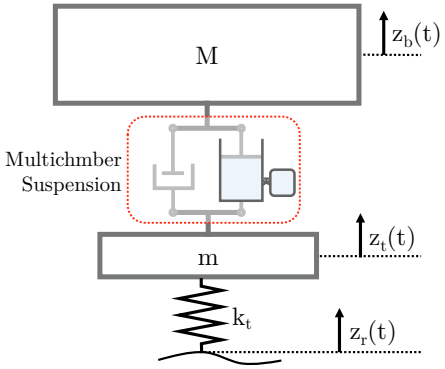

Fig. 4: Quarter car model representation

a quarter car equipped with a multichamber suspension is described by a 7^{th} order system with state variables

$$x(t) = [\, z_b(t)\ \dot{z}_b(t)\ z_t(t)\ \dot{z}_t(t)\ p_m(t)\ p_{aux}(t)\ c(t)\,]^T \tag{16}$$

and equations

$$\begin{aligned}
M\ddot{z}_b(t) =& -c(t)(\dot{z}_b(t) - \dot{z}_t(t)) + A(p_m(t) - p_{atm}) \\
& - Mg \\
m\ddot{z}_t(t) =& +c(t)(\dot{z}_b(t) - \dot{z}_t(t)) - A(p_m(t) - p_{atm}) + \\
& + Mg - k_t(z_t(t) - z_r(t)) \\
\dot{p}_m(t) =& -\frac{np_m(t)A(\dot{z}_b(t) - \dot{z}_t(t))}{V_m(t) + s(t)V_{aux}} \\
\dot{p}_{aux}(t) =& -\frac{np_{aux}(t)A(\dot{z}_b(t) - \dot{z}_t(t))}{V_m(t) + V_{aux}} s(t) \\
\dot{c}(t) =& -\beta c(t) + \beta c_{in}(t).
\end{aligned} \tag{17}$$

The discontinuous nature of the model is accounted for by the state reinitialization every time the control valve switches:

$$\begin{aligned}
&\text{if } s(\bar{t}^-) = 0 \wedge s(\bar{t}^+) = 1 \quad \rightarrow x_0 = \begin{bmatrix} x_1(\bar{t}^-) \\ x_2(\bar{t}^-) \\ x_3(\bar{t}^-) \\ x_4(\bar{t}^-) \\ p^{eq}(\bar{t}^-) \\ p^{eq}(\bar{t}^-) \\ x_7(\bar{t}^-) \end{bmatrix} \\
&\text{if } s(\bar{t}^-) = 1 \wedge s(\bar{t}^+) = 0 \quad \rightarrow x_0 = x(\bar{t}^-).
\end{aligned} \tag{18}$$

One of the inputs of the quarter-car model is the road profile. In this paper, we model the road following the standard ISO8608 and adopting the analytical formulation, proposed by Agostinacchio et al. (2014).

$$z_r(x) = \sum_{i=0}^{N} \sqrt{\Delta n}\ 2^k 10^{-3} \left(\frac{n0}{i\Delta n}\right) \cos\left(2\pi\ i\Delta n\ x + \varphi_i\right) \tag{19}$$

where x is the spatial variable from 0 to $L = 10\ km$; $\Delta n = 1/L$; $n_{max} = 1/B$; B is the sampling space interval; $N = L/B$; $n_0 = 0.1\ cycles/m$; $\varphi_i \in [0, 2\pi]$ is a random phase; k is a natural number that depends on the road profile class, for a class C-D, we used $k = 5$.

3. COMFORT ORIENTED OPTIMIZATION

We assess the potential of the multichamber architecture to improve ride comfort by setting an optimization problem. Since the objective is that to define the maximum performance that the architecture can achieve, we adopt the following assumptions:

Assumption 4. The requested damping $c_{in}(t)$ is defined by the mixed SH-ADD control algorithm (see Savaresi and Spelta (2007)) that has been shown to approach the filtering limit of a semi-active suspension.

Assumption 5. The performance is quantified by the sprung mass vertical acceleration mean square (see (ISO 2631-1:1997):

$$J = \frac{1}{T}\int_{t_0}^{t_0+T} \ddot{z}_b^2(t)dt \tag{20}$$

Assumption 6. The road disturbance $z_r(t)$ is known. In other words, a perfect preview of the road profile is assumed to be available: the current valve state can be chosen based on the knowledge of the future disturbance.

Assumption 7. The control strategy sampling period is T_r.

Assumption 8. A receding horizon approach is adopted. The optimization is carried out in a *time window* of duration $T_w = T_r Q$, where $Q \in \mathbb{N}$. Then the optimal sequence is applied for the first *time step* T_r, and the optimization problem is solved again in a time window T_w shifted ahead of a *time step* T_r.

Assumption 7 and Assumption 8 entail that Q is the number of optimization variables in a *time window*: the optimization result is the valve state in each *time step*: s_τ where $\tau = 1, 2, ..., Q$.

We specialize the above problem in three versions considering different switching limitations. The first optimization problem is called *Unconstrained Optimization*; it allows for an unconditional valve switching. In practice, there are not constraints that forbid a valve opening or closing. The second optimization problem, termed *Opening Constrained Optimization*, introduces a constraint for the valve opening: a valve opening can occurs only if the difference between the pressure in the main chamber and the pressure in the auxiliary chamber is lower than a threshold $\overline{\Delta P}$. The third optimization problem, the *Switching Constrained Optimization*, further constraints the valve switching to switch only if the suspension stroke is lower than $\overline{\Delta z}$. The switching constraints are designed to avoid the non-idealities described in Section 2.2 and represent possible strategies that could be implemented to minimize pressure kicks and static force drifts.

3.1 Unconstrained Optimization

The Unconstrained Optimization is formalized as

$$\begin{aligned}
&\min_{\substack{s_\tau \\ \tau = 1, ..., Q}} \quad \frac{1}{T_w}\int_{t_0}^{t_0+T_w} \ddot{z}_b^2(t)dt \\
&\text{subject to (17).}
\end{aligned} \tag{21}$$

Since the optimization variable is a two state discrete variable ($s_\tau \in \{0,1\}$), in each *time window* the number N of possible valve state sequences $s(t)$ is $N = 2^Q$. This makes a receding horizon exhaustive search viable, yielding the following approach:

(i) $t_0 = 0$.
(ii) If $t_0 > T_H$, then exit.
(iii) Test all the 2^Q sequences of $s(t)$, simulating equations (17) starting from $x_0 = x(t_0)$, for $t \in [t_0, t_0 + T_w]$.
(iv) Choose the sequence $s_{opt}(t)$ that generates the minimum cost function J.
(v) Apply the optimal sequence $s_{opt}(t)$ for $t \in [t_0, t_0+T_r]$.
(vi) Set $t_0 = t_0 + T_r$.
(vii) Return to (ii).

where T_H is the simulation horizon. The applied sequence is the solution of the optimization problem. The unconstrained optimization represents the best achievable performance considering the above assumptions.

3.2 Opening Constrained Optimization

The *Opening Constrained Optimization* is obtained starting from the unconstrained case described in (21), and introducing a constraint on the valve opening: if the absolute value of the pressure difference is greater than threshold $\overline{\Delta p}$ at $t = \bar{t}$, then the valve cannot be opened at that time instant.

This constraint has been introduced for two different reasons. The first one is related to the model uncertainty; the multichamber model is derived under Assumptions 1 and 2, in practice the mass flow through the air-spring valve is not modelled. The higher the pressure difference is, the larger the mass flow through the valve, then the more significant is the neglected phenomenon. Limiting the valve opening only when the pressure difference is lower than a threshold, means to limit the region in which the model is not accurate. The second reason is related to the generation of kick forces; when the valve is opened, the higher the pressure difference is, the higher the kick force generated.

The algorithm used for the solution of this optimization problem is a simple evolution of the algorithm implemented for the unconstrained case: in the exhaustive search only the sequences that does not violate the constraint are explored and evaluated.

3.3 Switching Constrained Optimization

In this case, the valve can switch only if the absolute value of the stroke is smaller than a threshold $\overline{\Delta z}$. The constraint on the valve switching has been introduced in order to preserve the static position. Consider the ideal case in which the valve is switched always in the static position $z_b(t) - z_t(t) = 0$, this switching strategy guarantees that the static position does not change, since the static position is the intersection of the two passive stiffness characteristics (see Figure 2). Moreover, switching in the same position guarantees that the pressure in the two chambers is the same thus avoiding kick forces. It is a stricter constraint than the one on the valve opening only.

Model Parameters	**Symbol**	**Value**
Sprung mass	M $[kg]$	785
Unsprung mass	m $[kg]$	50
Tire stiffness	k_t $[N/mm]$	250
Maximum damping	c_{max} $[Ns/mm]$	4.3
Minimum damping	c_{max} $[Ns/mm]$	0.9
Damping bandwidth	β $[rad/s]$	$2\pi 40$
Main chamber initial pressure	p_{m0} $[bar]$	8.05
Aux. chamber initial pressure	p_{aux0} $[bar]$	8.05
Main chamber initial volume	V_{m0} $[l]$	2.354
Aux. chamber volume	V_{aux} $[l]$	1.085
Piston area	A $[m^2]$	0.011
Adiabatic coefficient	n [ ]	1.36

Table 1: Numerical values of parameters used in simulation

The algorithm used for the solution of this optimization problem is the same used for the *Opening Constrained Optimization Problem*: the optimal sequence is chosen among the sequences that do not violate the constraint.

4. OPTIMIZATION RESULTS

This section analyses the results of the three algorithms and compares them against the best comfort-oriented policy: open air-spring valve (yielding the softest passive configuration) and mixed SH-ADD damping control (state of the art solution for the comfort oriented semi-active damping control). Tab. 1 summarizes the model parameters. In all the following simulations, the car is driven straight at a constant speed of $V_x = 20$ m/s.

The optimization is solved with $T_w = 300$ ms (which corresponds to a 6 m preview at $V_x = 20$ m/s). This window is long enough to endow the control system with the proper amount of preview to yield close to optimal results. The role of *Time Step* which depends on the actuator bandwidth, is studied through a sensitivity analysis.

We quantify the performance of the architecture by defining a relative *improvement index*

$$J_{imp} = \frac{J^* - J_{ref}}{J_{ref}} \ 100 \tag{22}$$

where: J^* is the comfort index obtained simulating the stiffness control sequence; J_{ref} is the comfort index obtained with the softest spring configuration (open valve). By definition, if $J_{imp} < 0$, the control sequence improves the comfort with respect to the passive configuration.

Figure 5 presents the results of the *Unconstrained Optimization* as a function of *Time Step* T_r. From figure, one concludes that:

- the multichamber suspension algorithm outperforms the current state-of-the-art for all T_r.
- The relationship between J_{imp} and T_r is monotonic: the lower the *Time Step* is, the greater the improvement with respect to the passive configuration. The improvement obtained with a slow valve ($T_r = 100$ ms) is -7.1%, while with a fast valve ($T_r = 20$ ms) the improvement is -16.7%. The case of $T_r = 30$ ms has been used for the solution of the two constrained op-

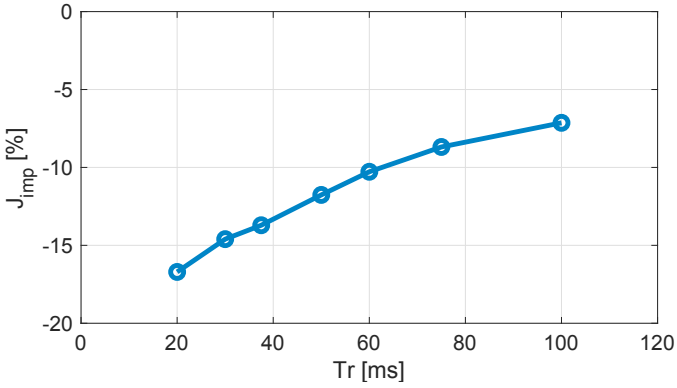

Fig. 5: Unconstrained optimization problem result

timization problems, it represents the switching time of the valve used in standard semi-active suspensions.

We now introduce the switching constraints. Figure 6 plots the sensitivity of the *Opening Constrained Optimization* to the threshold $\overline{\Delta P}$ and the performance of the *Opening Constrained Optimization* with $\overline{\Delta z} = 5$ mm. The figure shows that,

- the stricter the constraint is, the worse the results are.
- Up to $\overline{\Delta P} = 1.5$ bar, the performance of the constrained approach are not too far from the benchmark. This means that the unconstrained optimization already tries to avoid switching when there is a large pressure difference.
- Even in case of $\overline{\Delta P} = 0.5$ bar there is a significant improvement: -9.7%.
- The *Opening Constrained Optimization* yields an improvement of less than 2%. The $\overline{\Delta z} = 5$ mm threshold on the position guarantees that there are no valve opening with a pressure difference greater than 0.5 bar.

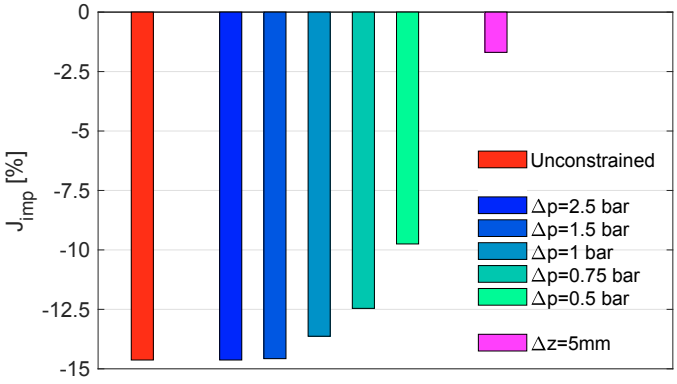

Fig. 6: Summary of the optimization results

Remark. As previously discussed, the passive air-spring benchmark is the open valve one. This configuration, while being the best passive solution for the steady driving comfort, cannot be employed in practice; indeed, during dynamic manoeuvrers, *i.e.* braking and turning, it would yield large pitch and roll movements. It is thus of interest to compare the proposed approach also with the performance of the closed-valve air-spring, whose stiffness value is more suitable to be employed in a realistic passive spring scenario. The comfort index obtained in this case is $J_{imp} = +48.13\%$; such result allows to stress even more the potential benefits of using the controlled multichamber suspension in a real application.

5. CONCLUSIONS

This paper discusses the modelling and comfort oriented performance benchmarking of a multichamber suspension. Designed so to allow a fast modulation of the spring stiffness, multichamber suspensions are hardly modelled as ideal reactive suspensions: the pressure dynamics in the chambers call for special care both in modelling and control.

We propose to consider these features by designing a full knowledge optimal control. The optimal strategy confirms that while the potential of improvements is considerable (up to 16%), the effects the suspension state (and in particular the pressure in the chamber) has on the switching dynamics cannot be neglected. In fact, by imposing the switch to happen only when the stroke is close to the nominal value only leads to a 2% improvement. Accounting for the chamber pressure is paramount to achieve good performance.

Future works will focus on the design of a real-time closed loop control strategy for the multichamber suspension.

REFERENCES

Agostinacchio, M., Ciampa, D., and Olita, S. (2014). The vibrations induced by surface irregularities in road pavements – a matlab® approach. *European Transport Research Review*, 6(3), 267–275.

Anubi, O.M. and Crane, C. (2015). A new semiactive variable stiffness suspension system using combined sky-hook and nonlinear energy sink-based controllers. *IEEE Transactions on Control Systems Technology*, 23(3), 937–947. doi:10.1109/TCST.2014.2353303.

ISO 2631-1:1997 (1997). Mechanical vibration and shock – evaluation of human exposure to whole-body vibration general requirements. Standard, International Organization for Standardization.

Savaresi, S., Poussot-Vassal, C., Spelta, C., Sename, O., and Dugard, L. (2010). *Semi-Active Suspension Control Design for Vehicles*. Butterworth-Heinemann.

Savaresi, S. and Spelta, C. (2007). Mixed sky-hook and add: Approaching the filtering limits of a semiactive suspension. *Journal of Dynamic Systems Measurement and Control-transactions of The Asme - J DYN SYST MEAS CONTR*, 129. doi:10.1115/1.2745846.

Spelta, C., Previdi, F., Savaresi, S., Bolzern, P., Cutini, M., Bisaglia, C., and Bertinotti, S. (2011). Performance analysis of semi-active suspension with control of variable damping and stiffness. *Vehicle System Dynamics - VEH SYST DYN*, 49, 237–256. doi: 10.1080/00423110903410526.

Youn, I. and Hac, A. (1995). Semi-active suspensions with adaptive capability. *Journal of Sound and Vibration*, 180(3), 475 – 492. doi: https://doi.org/10.1006/jsvi.1995.0091.